Compared vulnerabilities to small cardiac motions between different cameras used for myocardial perfusion imaging

Julien Salvadori, PhD,[a] Yolande Petegnief, PhD,[b] Remi Sabbah, MD,[b] Olivier Morel, MD,[b] Hatem Boulahdour, MD, PhD,[b] Gilles Karcher, MD, PhD,[c,d] Pierre-Yves Marie, MD, PhD,[c,d,e] and Laetitia Imbert, PhD[a,c,f,g]

[a] Institut de Cancérologie de Lorraine, Université de Lorraine, Nancy, France
[b] CHU-Besançon, Université de Franche-Comté, Service de Médecine Nucléaire, Besançon, France
[c] CHRU-Nancy, Université de Lorraine, Plateforme Nancyclotep, Nancy, France
[d] Médecine Nucléaire, Hôpital de Brabois, CHRU-Nancy, Université de Lorraine, Service de Médecine Nucléaire, Nancy, France
[e] Université de Lorraine, INSERM, UMR-1116 DCAC, Nancy, France
[f] Université de Lorraine, INSERM, UMR-947 IADI, Nancy, France
[g] Médecine Nucléaire, Hôpital de Brabois, CHRU-Nancy, Nancy, Vandœuvre-lès-Nancy, France

Received Oct 10, 2017; accepted Dec 8, 2017
doi:10.1007/s12350-017-1175-6

This phantom-based study was aimed to determine whether cardiac CZT-cameras, which provide an enhanced spatial resolution and image contrast compared to Anger cameras, are similarly affected by small cardiac motions. Translations of a left ventricular (LV) insert at half-SPECT acquisitions through six possible orthogonal directions and with 5- or 10-mm amplitude were simulated on the Discovery NM-530c and DSPECT CZT-cameras and on an Anger Symbia T2 camera equipped with an astigmatic (IQ.SPECT) or conventional parallel-hole collimator (Conv.SPECT). SPECT images were initially reconstructed as currently recommended for clinical routine. The heterogeneity in recorded activity from the 17 LV segments gradually increased between baseline and motions simulated at 5- and 10-mm amplitudes with all cameras, although being higher for Anger- than CZT-cameras at each step and resulting in a higher mean number of artifactual abnormal segments (at 10-mm amplitude, Conv.SPECT: 3.7; IQ.SPECT: 1.8, Discovery: 0.7, DSPECT: 0). However, this vulnerability to motion was markedly (1) decreased for Conv.SPECT reconstructed without the recommended Resolution Recovery algorithm and (2) increased for DSPECT reconstructed without the recommended cardiac model. CZT-cameras and especially the DSPECT appear less vulnerable to small cardiac motions than Anger-cameras although these differences are strongly dependent on reconstruction parameters. (J Nucl Cardiol 2019;26:1313–22.)

Key Words: CZT-cameras • anger-cameras • myocardial perfusion imaging • patient motions • artifacts

Electronic supplementary material The online version of this article (https://doi.org/10.1007/s12350-017-1175-6) contains supplementary material, which is available to authorized users.

The authors of this article have provided a PowerPoint file, available for download at Springer Link, which summarises the contents of the paper and is free for re-use at meetings and presentations. Search for the article DOI on SpringerLink.com.

Reprint requests: Laetitia Imbert, PhD, Médecine Nucléaire, Hôpital de Brabois, Allée du Morvan, 54500, Nancy, Vandœuvre-lés-Nancy, France; *l.imbert@chru-nancy.fr*

1071-3581/$34.00

Copyright © 2018 American Society of Nuclear Cardiology.

Abbreviations

Conv.SPECT	Conventional SPECT
CZT	Cadmium–Zinc–Telluride
DNM 530c	Discovery NM530c
FBP	Filtered back projection
FWHM	Full width at half maximum
IQ	Interquartile range
LEHR	Low-energy high resolution
LV	Left ventricle
OSEM	Ordered subset expectation maximization
RR	Resolution recovery
SPECT	Single photon emission computed tomography

See related editorial, pp. 1323–1326

INTRODUCTION

Patient motions constitute a frequent source of artifacts for myocardial perfusion SPECT imaging. The incidence of detectable motions can reach levels ranging from 25 to 35% in clinical routine[1–3] although only a small proportion of these motions is considered to lead to significant artifacts depending on their amplitude, direction and position during the scan.[1,2,4–11] In a general manner, it is well known that large motions of two pixels or more (> 10 mm) potentially lead to significant artifacts[2,4,12] and require being detected by adapted tools such as sinograms and linograms, with the current recommendation that they justify at least a motion correction (guidelines of the European Association of Nuclear Medicine[13]). The same recommendations may not be applied for the smaller motions which are more difficult to detect and correct, although their influence on image interpretation cannot be neglected.

Both Anger- and CZT-cameras are likely to benefit from modern reconstruction systems in clinical routine, with a 3D-modeling of the beam allowing improving spatial resolution and image contrast. However, the question arises as to whether the vulnerability to cardiac motions, and especially to small motions, is the same for the more recent CZT cameras for which tomographic spatial resolution is clearly enhanced comparatively to Anger-cameras, reaching a level of approximately 6 to 9 mm.[14] These CZT cameras also provide a definite enhancement in image contrast[14] and these properties are likely to have an influence on the production and detectability of motion-related artifacts.

In light of the above, this phantom-based study was aimed at determining the extent to which the Discovery NM-530c and DSPECT cardiac CZT cameras are vulnerable to small cardiac motions when used with their recommended reconstruction processes, as well as their respective comparison in this setting with Anger cameras equipped with either an astigmatic or a conventional parallel-hole collimator.

MATERIALS AND METHODS

Cameras and Systems

This study was performed on (1) the two currently commercialized CZT-cameras dedicated to nuclear cardiology, the Discovery NM 530c (General Electric Healthcare)[15–17] and the DSPECT (Spectrum Dynamics),[18–20] as well as (2) the Symbia T2 Anger camera (Siemens Medical Solutions) equipped with an astigmatic collimator (IQSPECT)[21,22] or with a high-resolution parallel-hole collimator (Conv.SPECT).

SPECT Acquisitions and Simulated Cardiac Translations

A simple cardiac phantom, mimicking the shape of a normal left ventricle (Biodex Medical Systems, see Figure 1), was used. The left ventricular walls were filled with a 10 MBq solution of ^{99m}Tc and the left ventricular cavity was filled with water. This phantom was orientated with two 45° tilts for the left-anterior-oblique and head-to-feet directions, respectively (Figure 1).

SPECT data were acquired for each of the four cameras, first at baseline, at the center of the field of view, and secondly after the phantom had been translated with amplitudes of 5 or 10 mm along the *X* or *Y* transaxial directions or along the *Z* axis longitudinal direction (the three axes are depicted in Figure 1). One translation-direction was obtained with the mechanisms of bed elevation and the two others, with careful manual displacements on a horizontal printed target. These translations were additionally applied in a positive or negative direction, resulting in a total of six possible directions (i.e., $-X/+X$, $-Y/+Y$ and $-Z/+Z$). For each camera, time-per-projection was set to target the recording of 500 myocardial *k* counts while the reconstruction parameters, detailed in Table 1, were those recommended for clinical routine. Additionally, certain changes in reconstruction parameters were also tested, namely, (1) the suppression of the cardiac model-based system for DSPECT and (2) for Conv.SPECT, the switch from the recommended OSEM method incorporating a Resolution Recovery algorithm (OSEM-RR, see parameters in Table 1) to a less sophisticated OSEM reconstruction method (Eight iterations, four subsets) associated with a Gaussian filter (full-width at half maximum of 10 mm) or to a filtered back projection (FBP) associated with a Butterworth filter (order 5, cut frequency 0.55).

Only the SPECT projections, involving a unidirectional translation at half acquisition, were simulated. For each camera, the SPECT projections, from the first half of the baseline untranslated acquisition, were combined with those from the second half of each translated acquisition in a new set of SPECT projections.

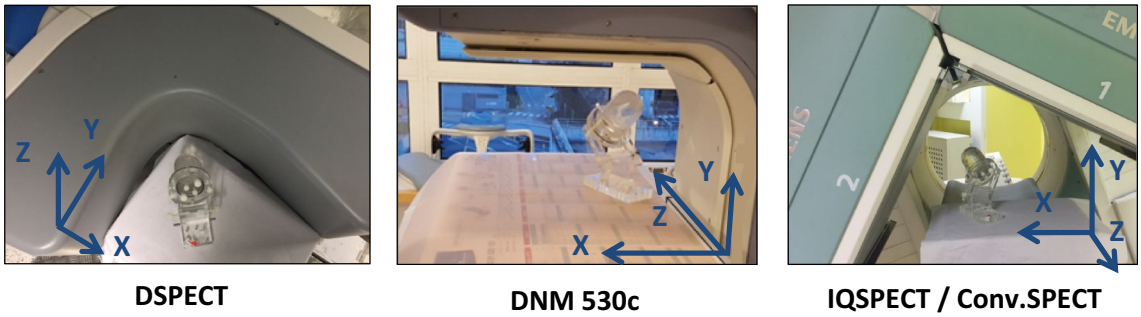

Figure 1. Representations of the three orthogonal axes (*X*, *Y*, and *Z*) and of the orientation and placement of the left ventricular insert at the center of the field of view at baseline, prior to any translation, for the DSPECT (left panel) and Discovery NM530c (middle panel) CZT-cameras and for the Symbia Anger-cameras (right panel, IQSPECT/Conv.SPECT).

In addition, reconstructed SPECT images from translated and non-translated acquisitions were merged in a same set of 3D fusion images to provide a comprehensive visualization of the respective positions of the left ventricular walls before and after translations.

Analyzed Parameters

For each of the four cameras, the analyses involved the single set of SPECT-images obtained at baseline, without any translation, and the 12 different sets of SPECT-images produced for simulated motions occurring at half acquisitions [i.e., corresponding to the product of the three directions (*X*, *Y*, and *Z*), both negative and positive, and with the two amplitudes (5 and 10 mm)]. SPECT images were represented with polar maps and the segmental activities were determined with a 17-segment left ventricular model and the Quantitative Perfusion SPECT software from the Cedars-Sinai Medical Center.[23]

The distribution of segmental activities was represented for each of the four cameras with three plot-boxes corresponding respectively to segments from baseline SPECT ($n = 17$) and to a mixing of segments from all SPECT simulating motions of 5-mm ($n = 102$) or 10-mm amplitude ($n = 102$).

The ranges between the upper and lower limits of the plot-boxes (with the exclusion of outliers), as well as the interquartile range (IQ, corresponding to the difference between the upper and lower quartiles), were used for assessing the homogeneity in segmental activities of each camera.

Definitely abnormal segments were defined by a $< 65\%$ uptake, a threshold currently used to identify areas of significant myocardial infarction at rest-SPECT.[24–26]

Statistical Analysis

Segmental activities were expressed as median and interquartile range. Two-group comparisons were performed with non-parametric Mann–Whitney tests. Differences with a $P < .05$ were considered to be statistically significant.

RESULTS

Baseline SPECT Images

In the absence of any simulated motion, there was no abnormal segment detected with any of the cameras, with all segmental activities higher than 65%. However, the distribution of segmental activities was more heterogeneous with Anger-cameras comparatively to CZT-cameras and especially comparatively to the DSPECT, as evidenced by the plot-boxes displayed in Figure 2 and values from Table 2. Respective interquartile ranges were 9.9% for Conv.SPECT, 9.1% for IQ.SPECT, 7.0% for Discovery and 4.8% for DSPECT.

These heterogeneities were characterized by lower relative uptakes for septal, apical and lateral segments, when compared with anterior and inferior segments, as evidenced on polar maps in Figure 3. The differences in activities between these two segment groups were notable for IQ.SPECT (respective median values: 77.3% vs 88.6%, $P = .001$) and for Conv.SPECT (75.6% vs 85.6%, $P = .001$), while less marked for Discovery (78% vs 85%, $P = .001$) and absent for DSPECT (81.8% vs 82.0%).

SPECT Images with Simulated Motions

As evidenced on polar maps in Figure 3, on plot-boxes in Figure 2 and on values in Table 2, the heterogeneity in segmental activities increased gradually between baseline and motions simulated at 5- and 10-mm amplitudes with a progressive widening of the interquartile ranges with all cameras. However, this heterogeneity remained higher for Anger cameras than for CZT cameras at both 5- and 10-mm amplitudes. At 10-mm amplitude, respective interquartile ranges were 12.0% for Conv.SPECT, 11.3% for IQ.SPECT, 10.0% for Discovery, and 8.0% for DSPECT.

Table 1. Acquisition and reconstruction parameters recommended for clinical routine for each tested camera

	DSPECT	Discovery-NM530c	IQSPECT	Conventional-SPECT
Acquisition parameters				
Collimator	Wide-angle parallel hole	Multipinhole	Astigmatic	LEHR parallel hole
Matrix size	64 × 64	32 × 32	128 × 128	64 x 64
Pixel size	4.92 mm	2.46 mm	4.8 mm	6.6 mm
Energy window	140 keV ± 10%	140 keV ± 10%	140 keV ± 7.5%	140 keV ± 7.5%
Number of projections	120 (× 9 blocks)	19	17 (× 2 heads)	16 (× 2 heads)
Detector angle between consecutive projections	0.4°-7°[a]	None (fixed detector)	6°	3°
Reconstruction parameters				
Method	ML-EM (OSEM[20])	MAP-EM (OSL)[17]	Conjugate Gradient Iterative Reconstruction[21]	OSEM with Resolution Recovery (Flash3D[28])
Number of iterations	7	50	10	8
Number of subsets	32	1	3	4
Inter-iteration filter	Kernel (0.125) Cardiac filter	-	-	-
Final filter	Normalizing filter[b]	Butterworth (order 7, cut-off: 0.37 cm^{-1})	Gaussian (10 mm FWHM)	Gaussian (10 mm FWHM)
Central tomographic spatial resolution (mm)[c]	6.7	8.6	15.0	13.5

FWHM, full width at half maximum; *LEHR*, low-energy high resolution

[a]Angles are approximately 0.4° for projections passing through the cardiac region (as defined by an adjusted region of interest on pre-scan images) and up to 7° for the other projections

[b]The normalizing filter leads to lower voxel values higher than 80% of maximal value by means of a gamma fit, in order to remove hot spots from normal myocardial areas[19,20]

[c]Assessed using the full width at half maximum of a linear source

Consequently, the inferior limit of certain plot-boxes fell below the 65% level (Figure 2), resulting in the detection of artifactual abnormal segments. At an amplitude of 5-mm, such abnormal segments were documented with only Conv.SPECT (mean number of abnormal segments per SPECT acquisition: 2.2) whereas at 10-mm, abnormal segments were documented for Conv.SPECT, IQ.SPECT, and Discovery (mean number of abnormal segments per SPECT acquisition: 3.7, 1.8, and 0.7, respectively).

Changes in Reconstruction Methods

When the recommended cardiac model was excluded from the DSPECT reconstruction process, the SPECT images became much more heterogeneous and significant artifacts were revealed with stimulated motions (Figure 4 and Table 2). Indeed, this model allows concentrating the myocardial signal around a center line, within the wall thickness, thereby opposing the dispersion of the signal generated by the walls.

On the contrary, for conventional SPECT, the heterogeneity in segmental activities was markedly lowered when FBP or OSEM was used instead of the recommended OSEM-RR method (Figure 4 and Table 2).

Analyses According to Translation Direction

As evidenced by polar maps in Figures 3 and 4, the observed heterogeneities in segmental activities were limited for motions along the longitudinal *z*-axis and more marked for motions in the axial *X* and *Y* directions, except for DSPECT reconstructed with the cardiac model and Conv.SPECT reconstructed without the RR algorithm (FBP and OSEM in Figure 4) which were all weakly vulnerable to motion, regardless of motion direction. In addition, the Discovery NM 530c had the particularity of being less sensitive to the axial motions when simulated in the *Y* rather than *X* direction (Figure 3).

Fusions of the reconstructed SPECT images, obtained at baseline and after 10-mm translations, are displayed in Figure 5, providing a clear visualization of the translation directions according to the doubled aspect of the walls. This double-wall aspect is mostly detectable with the CZT-cameras for which spatial resolution is sufficiently high for this purpose. These translation directions, identified by red arrows on the CZT-SPECT images in Figure 5, point in the same directions as those indicated by the corresponding arrows on the polar-maps obtained with 10-mm motions in Figures 3 and 4.

In this manner, it can be observed that the walls showing the lowest activities after 10-mm motion were roughly orientated orthogonal to these translation directions, except for the camera and methods that were weakly vulnerable to cardiac motion [DSPECT with the cardiac model (Figure 3) and Conv.SPECT with OSEM or FBP (Figure 4)]. This correspondence was particularly manifest for the DSPECT reconstructed without the cardiac model (Figure 4) and somewhat less for Discovery NM-530c and especially for Anger-cameras with Conv.SPECT reconstructed with the OSEM-RR methods (Figure 3). In these latter instances, the sites with low activities were (1) notably absent for motion in the *Z* direction and (2) closer to the centers of the septal and lateral walls for motions in the axial *X* and *Y* directions.

DISCUSSION

Based on our phantom experiments, the CZT-cameras and especially the DSPECT appear less vulnerable to small cardiac motions than Anger-cameras, in spite of the fact that higher spatial resolutions are achieved with the CZT-cameras.[14] However, this finding is mostly explained by differences in the preexisting homogeneity at baseline and above all, in SPECT reconstruction methods.

In the present study, definitely abnormal segments, with an activity $< 65\%$, were rather uncommon with motions of only 5-mm amplitude, but were much more frequent for motions of 10-mm amplitude, especially with Anger-SPECT, reaching a mean number of abnormal segments of 3.4 for conventional-SPECT and 1.8 for IQ-SPECT when using recommended reconstruction methods. As evidenced by the plot boxes in Figure 2, these abnormal segments were linked to the motion-related increase in the heterogeneity of segmental uptake, with marked increases in interquartile ranges and marked decreases in the inferior limits of the plot boxes for both Anger- and CZT-cameras. However, the level of heterogeneity was already higher at baseline for the Anger-cameras, prior to any simulated motion. Thus, this preexisting difference likely explained the higher heterogeneities observed with the Anger-cameras with further deteriorations due to simulated motions (Figure 2).

The activity recorded from our insert at baseline was somewhat lower for the septal, apical, and lateral walls, especially for the Anger-cameras and primarily for conventional SPECT reconstructed with OSEM-RR as already observed in a previous study.[27] As a result, several segments were identified as definitely abnormal when additional decreases in septal and/or lateral signal were produced by certain simulated motions, namely those with translations oriented close to the orthogonal

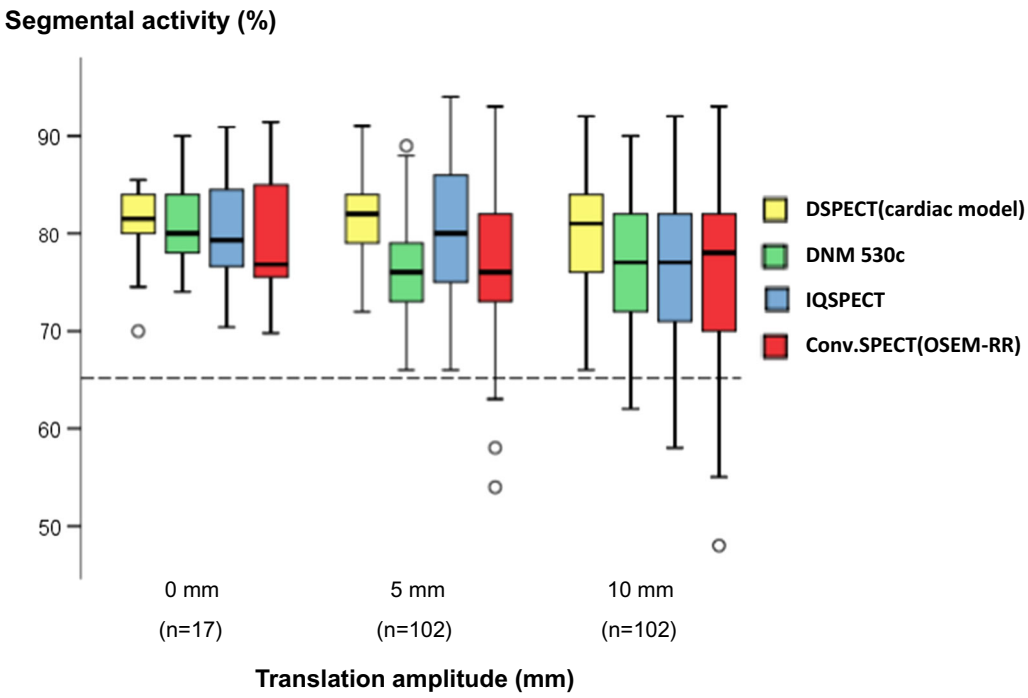

Figure 2. Plot boxes showing, for each of the four cameras, the distribution of segmental activities at baseline and for motions simulated with 5- and 10-mm translations. The dashed line represents the limit used for defining a definite decrease in recorded activity (< 65% of maximal activity). Only the currently recommended methods of reconstruction were used in this instance (the cardiac model for the DSPECT and OSEM-RR for conventional SPECT).

Table 2. Median values (and interquartile range) for the segmental activities recorded with the different cameras and reconstruction methods and for baseline and simulated motions of 5- and 10-mm amplitudes

	Baseline	5-mm	10-mm
Recommended reconstruction methods			
DSPECT with cardiac model	81.5 (4.8)	82.0 (5.0)	81.0 (8.0)
Discovery-NM530c	80.0 (7.0)	76.0 (6.0)	77.0 (10.0)
IQSPECT	79.3 (9.1)	80.0 (11.0)	77.0 (11.3)
Conv.SPECT with OSEM-RR	76.8 (9.9)	76.0 (9.0)	78.0 (12.0)
Additional reconstruction methods			
DSPECT without cardiac model	79.0 (5.0)	74.5 (6.0)	74.5 (7.0)
Conv.SPECT with FBP	84.0 (5.0)	86.0 (7.0)	82.0 (10.0)
Conv.SPECT with OSEM	86.0 (4.0)	84.0 (8.0)	80.0 (11.0)

axis of the septal and lateral walls, in the *X* or *Y* axial direction, as opposed to the translations in the longitudinal *Z* direction which are parallel to these walls. As evidenced by the analysis of Figure 5, the segments orthogonal to the translation direction corresponded to those exhibiting the greater distance between their pre- and post-translation positions (i.e., segments with a definite doubled aspect on fusion images), a condition that is associated with a high spatial dispersion of the recorded signal and that is likely to favor SPECT artifacts.

In the present analysis, currently recommended reconstruction methods were used in a first instance, since they were likely to provide, for each camera, a level of resolution that may be achieved with acceptable levels of noise and of signal heterogeneity. In a

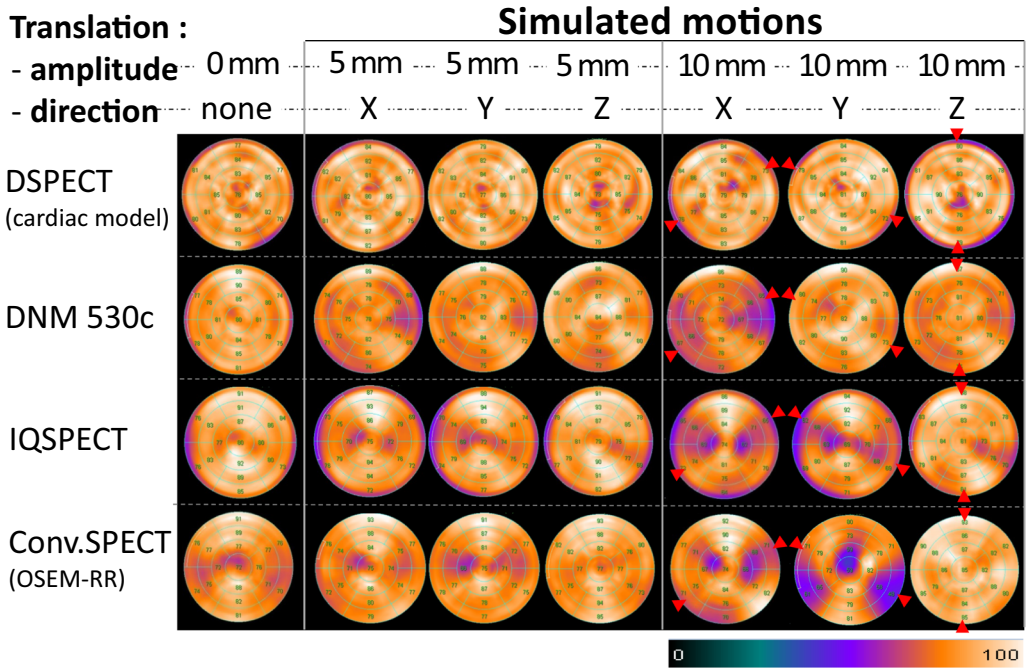

Figure 3. Polar maps of the SPECT images obtained with the four cameras using the recommended reconstruction parameters at baseline and for 5- or 10-mm translations in the positive *X*, *Y*, or *Z* directions. Red arrows, corresponding to the translation direction (see Figure 5), are additionally inserted on the polar-maps obtained with the 10-mm motions.

second step, however, we also show that very different results could be achieved with other reconstruction methods. This is firstly due to the use of the cardiac model that is commonly recommended with the iterative reconstruction process of the DSPECT camera. This model was found herein to be highly efficient in preventing heterogeneities in activity documented at baseline and especially with simulated motion (see polar maps obtained with and without the cardiac model in Figures 3 and 4, respectively). This model enables concentrating myocardial signals around a center line, within the wall thickness, thus opposing the spatial dispersion of the signal whereas such dispersion is likely to play a major role on motion-related artifacts.

This is secondly due to the use of a FBP or OSEM without RR as opposed to the OSEM-RR recommended reconstruction method for conventional SPECT, both FBP and OSEM alone being impossible to use with the other cameras. At the difference of the less sophisticated OSEM method, OSEM-RR involves the incorporation of a 3D-beam model, i.e., modeling of the spatial resolution of the collimator in order to restore an equivalent spatial resolution in the longitudinal and axial directions. OSEM-RR is likely to provide higher spatial resolution, lower noise and a reduction in image distortions when compared with FBP and OSEM-2D.[28] In our study, the central tomographic spatial resolution, assessed using the full width at half maximum for a linear source, was 11.7 mm with the recommended OSEM-RR reconstruction method applied on conventional SPECT but only 13.5 mm for OSEM without RR and 15.6 mm for FBP.

However, our results also show that OSEM-RR enhanced the vulnerability to cardiac motions as compared with FBP, strengthening a previously reported observation from another phantom-based study.[29] In the present study, this vulnerability was even higher with OSEM-RR than that observed for OSEM alone without the RR algorithm. This would suggest that the incorporation of the 3D-beam model is the main element likely to increase the vulnerability associated with the iterative reconstruction process of the conventional Anger-camera.

It may be additionally observed that areas of significant decreased activity were very scarce with motion along the longitudinal *Z* direction, even for the anterior and inferior walls, which are nonetheless oriented orthogonal to this direction (Figure 4) and contrary to that observed in a previous study, where a *Z* translation was also simulated on Anger-SPECT (simulation of diaphragmatic respiratory motions[30]). However, the translation-amplitudes leading to the presence of artifacts were higher in this previous study (2 cm). Furthermore, as previously discussed, the anterior and inferior walls were also those exhibiting the

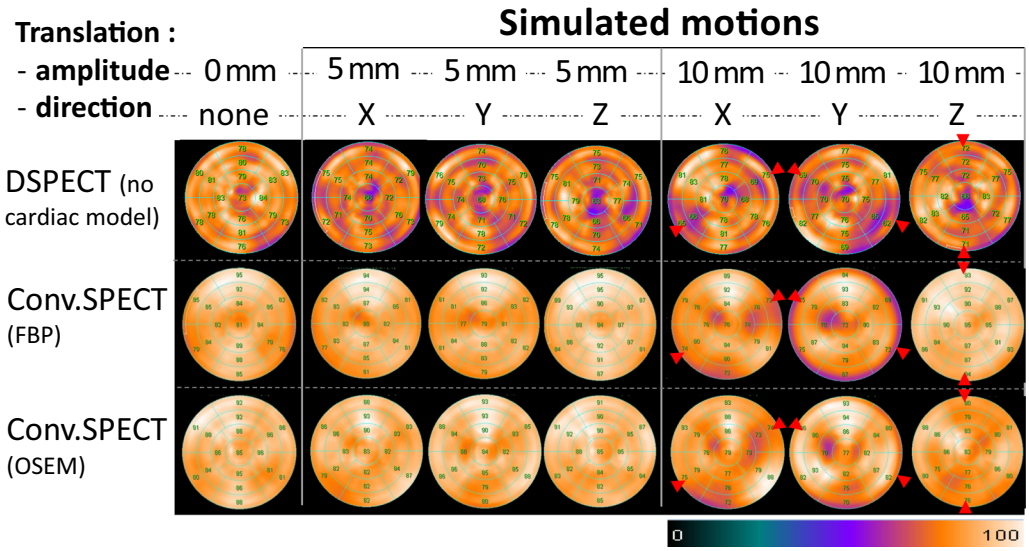

Figure 4. Polar maps of the SPECT images obtained at baseline and for 5- or 10-mm translations in the positive *X*, *Y*, or *Z* directions with the DSPECT camera after exclusion of the recommended cardiac model, and for conventional SPECT images reconstructed with OSEM without RR or FBP as opposed to the recommended OSEM-RR method. Red arrows, corresponding to the translation direction (see Figure 5), are additionally inserted on the polar-maps obtained with the 10-mm motions.

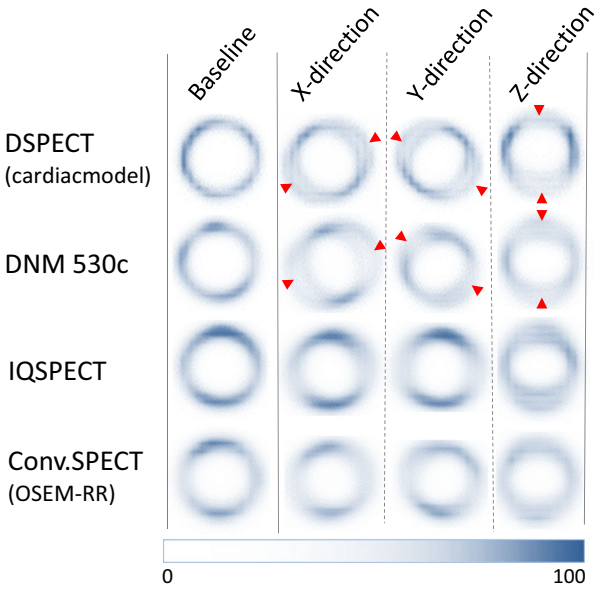

Figure 5. Midventricular short-axis slices obtained with each of the four cameras and recommended reconstruction methods: (1) at baseline, in the absence of any motion, and (2) with fusions of the two sets of reconstructed SPECT involved in each motion of 10-mm amplitude in the positive *X*, *Y*, or *Z* directions (i.e., fusion of the baseline non-translated SPECT-images with the SPECT-images obtained after the 10-mm translation). The CZT-SPECT images provide clear visualizations of the translation directions according to the areas showing the largest separations between the pre- and post-translation positions of the left ventricular walls (red arrows).

highest baseline activities with our recommended reconstruction methods, mainly for Anger-cameras and to a lesser extent for the Discovery NM 530c. As a result, motions along the *Z* direction were rather associated with a lowering of this excess in anterior and inferior activities, hence explaining the pattern of paradoxical homogeneity improvement, which was particularly manifest for the 10-mm *Z* translation with conventional SPECT reconstructed with the recommended OSEM-3D method (Figure 3).

A final novel observation was that the Discovery NM 530c had the particularity of being less vulnerable to the axial translations applied in the *Y* direction than to those applied in the *X* direction (see Figures 3, 5). A possible explanation is the asymmetrical geometry of this camera in which a displacement in the *X* direction will mainly affect five detectors aligned in this direction against four detectors for the *Y* direction. Lastly, the Discovery NM 530c was found to be mainly vulnerable to *Y* axial translations, the Anger cameras mainly vulnerable to *X* and *Y* axial translations and the DSPECT to all *X*, *Y*, and *Z* translations but only when the cardiac model was not included in the reconstruction process.

Certain limitations of this phantom-based study should be acknowledged, the first being that the clinical impact of the present findings remains to be assessed in a more extensive, in-depth manner. This impact is likely to depend on the relative effects of the small motions, as compared with other potential sources of local decreases

in recorded activity such as photon attenuation and physiological variations in myocardial thickness. The motion-related decreases in activity, when associated with the above additional sources of decreased activity in the same segments, possibly contribute toward attaining the lower activities corresponding to definitely abnormal segments.

Furthermore, the higher activities documented both herein and in a comparable study[27] on the inferior and anterior walls at baseline were not currently observed during in vivo SPECT imaging. This is presumably the result of the inferior and anterior signal being additionally lowered in vivo by diaphragmatic and breast attenuations and by breathing-related cardiac motions in the longitudinal Z axis.[30,31] The additional use of phantoms simulating these attenuations and motions could prove useful in this setting.

The impact of small motions on the sensitivity of the tests also needs to be assessed in vivo, with the consideration that the detectability of perfusion defects can vary according to their locations (i.e., with a possible enhanced detection in areas of motion-related decrease in recorded signal but not in other areas).

A final limitation is that the study did not include the use of methods developed for motion correction. However, these methods are recognized to be poorly adapted to such small motions and therefore, their application is currently not recommended in this setting.[13]

NEW KNOWLEDGE GAINED

(1) CZT-cameras are less vulnerable to small cardiac motions than Anger-cameras when reconstructed with currently recommended methods. (2) This vulnerability is particularly low for the DSPECT reconstructed with the recommended cardiac model. (3) This vulnerability is rather high for conventional Anger SPECT reconstructed with the recommended resolution recovery algorithm. (4) The myocardial segments orientated in a direction orthogonal to the translation direction are the more likely to exhibit motion artifacts.

CONCLUSION

The present study reveals that when reconstructed with the currently recommended methods, the CZT-cameras, and especially the DSPECT, are less vulnerable to small cardiac motions than Anger-cameras.

This lower vulnerability is observed in spite of the fact that higher spatial resolutions are achieved with the CZT-cameras, and is predominantly dependent on the choice of reconstruction parameters with: (1) a decreased vulnerability for Conv.SPECT reconstructed without the recommended Resolution Recovery algorithm and (2) an increased vulnerability for DSPECT reconstructed without the recommended cardiac model.

Finally, this study also yields evidence of a particular vulnerability to motion for segments imaged in a direction orthogonal to the translation direction and especially for those showing a decreased signal at baseline.

Disclosure

The authors declare that they have no conflict of interest.

References

1. Botvinick EH, Zhu YY, O'Connell WJ, Dae MW. A quantitative assessment of patient motion and its effect on myocardial perfusion SPECT images. J Nucl Med 1993;34:303-10.
2. Prigent FM, Hyun M, Berman DS, Rozanski A. Effect of motion on thallium-201 SPECT studies: A simulation and clinical study. J Nucl Med 1993;34:1845-50.
3. Wheat JM, Currie GM. Incidence and characterization of patient motion in myocardial perfusion SPECT: Part 1. J Nucl Med Technol 2004;32:60-5.
4. Cooper JA, Neumann PH, McCandless BK. Effect of patient motion on tomographic myocardial perfusion imaging. J Nucl Med 1992;33:1566-71.
5. Fitzgerald J, Danias PG. Effect of motion on cardiac SPECT imaging: Recognition and motion correction. J Nucl Cardiol 2001;8:701-6.
6. Friedman J, Van Train K, Maddahi J, Rozanski A, Prigent F, Bietendorf J, et al. ''Upward creep'' of the heart: A frequent source of false-positive reversible defects during thallium-201 stress-redistribution SPECT. J Nucl Med 1989;30:1718-22.
7. Sorrell V, Figueroa B, Hansen CL. The ''hurricane sign'': Evidence of patient motion artifact on cardiac single-photon emission computed tomographic imaging. J Nucl Cardiol 1996;3:86-8.
8. Wheat JM, Currie GM. Impact of patient motion on myocardial perfusion SPECT diagnostic integrity: Part 2. J Nucl Med Technol 2004;32:158-63.
9. Redgate S, Barber DC, Fenner Al-Mohammad A, Taylor JC, Hanney MB, et al. A study to quantify the effect of patient motion and develop methods to detect and correct for motion during myocardial perfusion imaging on a CZT solid-state dedicated cardiac camera. J Nucl Cardiol 2016;23:514-26.
10. Allie R, Hutton BF, Prvulovich E, Bomanji J, Michopoulou S, Ben-Haim S. Pitfalls and artifacts using the D-SPECT dedicated cardiac camera. J Nucl Cardiol 2016;23:301-10.
11. Kennedy JA, William Strauss H. Motion detection and amelioration in a dedicated cardiac solid-state CZT SPECT device. Med Biol Eng Comput 2017;55:663-71.
12. Matsumoto N, Berman DS, Kavanagh PB, Gerlach J, Hayes SW, Lewin HC, et al. Quantitative assessment of motion artifacts and validation of a new motion-correction program for myocardial perfusion SPECT. J Nucl Med 2001;42:687-94.
13. Hesse B, Tägil K, Cuocolo A, Anagnostopoulos C, Bardiés M, Bax J, et al. EANM/ESC procedural guidelines for myocardial perfusion imaging in nuclear cardiology. Eur J Nucl Med Mol Imaging 2005;32:855-97.

14. Imbert L, Poussier S, Franken PR, Songy B, Verger A, Morel O, et al. Compared performance of high-sensitivity cameras dedicated to myocardial perfusion SPECT: A comprehensive analysis of phantom and human images. J Nucl Med 2012;53:1897-903.
15. Buechel RR, Herzog BA, Husmann L, Burger IA, Pazhenkottil AP, Treyer V, et al. Ultrafast nuclear myocardial perfusion imaging on a new gamma camera with semiconductor detector technique: First clinical validation. Eur J Nucl Med Mol Imaging 2010;37:773-8.
16. Esteves FP, Raggi P, Folks RD, Keidar Z, Askew JW, Rispler S, et al. Novel solid-state-detector dedicated cardiac camera for fast myocardial perfusion imaging: Multicenter comparison with standard dual detector cameras. J Nucl Cardiol 2009;16:927-34.
17. Hebert T, Leahy R. A generalized EM algorithm for 3-D Bayesian reconstruction from Poisson data using Gibbs priors. IEEE Trans Med Imaging 1989;8:194-202.
18. Slomka PJ, Patton JA, Berman DS, Germano G. Advances in technical aspects of myocardial perfusion SPECT imaging. J Nucl Cardiol 2009;16:255-76.
19. Erlandsson K, Kacperski K, van Gramberg D, Hutton BF. Performance evaluation of D-SPECT: A novel SPECT system for nuclear cardiology. Phys Med Biol 2009;54:2635-49.
20. Gambhir SS, Berman DS, Ziffer J, Nagler M, Sandler M, Patton J, et al. A novel high-sensitivity rapid-acquisition single-photon cardiac imaging camera. J Nucl Med 2009;50:635-43.
21. Rajaram R, Bhattacharya M, Ding X, Malmin R, Rempel TD, Vija AH et al. Tomographic performance characteristics of the IQ-SPECT system. IEEE Nuclear Science Symposium and Medical Imaging Conference Record 2011.
22. DePuey EG. Advances in SPECT camera software and hardware: Currently available and new on the horizon. J Nucl Cardiol 2012;19:551-81.
23. Wolak A, Slomka PJ, Fish MB, Lorenzo S, Acampa W, Berman DS, Germano G. Quantitative myocardial-perfusion SPECT: Comparison of three state-of-the-art software packages. J Nucl Cardiol 2008;15:27-34.
24. Sciagrà R, Leoncini M, Marcucci G, Dabizzi RP, Pupi A. Technetium-99m sestamibi imaging to predict left ventricular ejection fraction outcome after revascularisation in patients with chronic coronary artery disease and left ventricular dysfunction: Comparison between baseline and nitrate-enhanced imaging. Eur J Nucl Med 2001;28:680-7.
25. De Geeter F, Franken PR, Knapp FF Jr, Bossuyt A. Relationship between blood flow and fatty acid metabolism in subacute myocardial infarction: A study by means of 99mTc-Sestamibi and 123I-beta-methyl-iodo-phenyl pentadecanoic acid. Eur J Nucl Med 1994;21:283-91.
26. Sciagrà R, Pellegri M, Pupi A, Bolognese L, Bisi G, Carnovale V, et al. Prognostic implications of Tc-99m sestamibi viability imaging and subsequent therapeutic strategy in patients with chronic coronary artery disease and left ventricular dysfunction. J Am Coll Cardiol 2000;36:739-45.
27. Liu CJ, Cheng JS, Chen YC, Huang YH, Yen RF. A performance comparison of novel cadmium–zinc–telluride camera and conventional SPECT/CT using anthropomorphic torso phantom and water bags to simulate soft tissue and breast attenuation. Ann Nucl Med 2015;29:342-50.
28. Zoccarato O, Scabbio C, De Ponti E, Matheoud R, Leva L, Morzenti S, et al. Comparative analysis of iterative reconstruction algorithms with resolution recovery for cardiac SPECT studies. A multi-center phantom study. J Nucl Cardiol 2014;21:135-48.
29. Kovalski G, Keidar Z, Frenkel A, Israel O, Azhari H. Correction for respiration artefacts in myocardial perfusion SPECT is more effective when reconstructions supporting collimator detector response compensation are applied. J Nucl Cardiol 2009;16:949-55.
30. Pitman AG, Kalff V, Van Every B, Risa B, Barnden LR, Kelly MJ. Effect of mechanically simulated diaphragmatic respiratory motion on myocardial SPECT processed with and without attenuation correction. J Nucl Med 2002;43:1259-67.
31. Roujol S, Anter E, Josephson ME, Nezafat R. Characterization of respiratory and cardiac motion from electro-anatomical mapping data for improved fusion of MRI to left ventricular electrograms. PLoS ONE 2013;8:e78852.